Dynamics of Odorant Binding to Thin Aqueous Films of Rat-OBP3

Masayuki Yabuki[1,2], David J. Scott[1], Loïc Briand[3] and Andrew J. Taylor[1]

[1]School of Biosciences, University of Nottingham, College Road, Sutton Bonington Campus, Loughborough, Leicestershire LE12 5RD, UK, [2]Perfumery Development, Global R&D, Kao Corporation, 2-1-3 Bunka Sumida-ku, Tokyo 131-8501, Japan and [3]Institut National Recherche Agronomique, Unite Mixte Recherche 1169 FLAVIC, F-21000, Dijon, France

Correspondence to be sent to: Andrew J. Taylor, School of Biosciences, University of Nottingham, College Road, Sutton Bonington Campus, Loughborough, Leicestershire LE12 5RD, UK. e-mail: andy.taylor@nott.ac.uk

Abstract

Uptake, retention and release of 5 selected odorants (benzaldehyde, 2-methylpyrazine, 2-isobutyl-3-methoxypyrazine, 2-isobutylthiazole, and 2,4,5-trimethylthiazole) by recombinant rat odor-binding protein 3 (rat-OBP3) were measured in a model system under nonequilibrium conditions. Gaseous odorants were introduced into a 100 mm section of a polar deactivated capillary in which aqueous rat-OBP3 films were formed to mimic the olfactory epithelium (OE), and the change in the gas-phase concentration of the outflow gas was monitored in real time using atmospheric pressure chemical ionization–mass spectrometry (APCI–MS). The 5 odorants were chosen because they exhibited a broad range of dissociation constants with rat-OBP3 and because they were amenable to detection by on-line APCI-MS. All 5 odorants were quantitatively bound by rat-OBP3, which resulted in an effective concentration of the odorants in the aqueous layer (about 50 000-fold). Odorant release from the rat-OBP3-odorant complex into the gas phase showed that odorant release was governed by the dissociation constant of the complex and the flow rate of odorant-free air. When 2 odorants were introduced into the system, odorant uptake and release were influenced by the method of introduction and their relative affinities for the protein. Because rat-OBP3 exhibits typical odorant-binding characteristics, the results not only provide fundamental information on the kinetics of odorant mass transfer induced by the presence of OBPs in the olfactory mucus layer but also support the possibility that vertebrate OBPs may facilitate the accumulation of odorants in the OE.

Key words: APCI-MS, capillary, in vitro, mass transfer, odorant-binding protein, olfactory mucus, peri-receptor

Introduction

In vertebrates, the initial stage of the olfaction process involves several interlinked mass transfer processes. Initially, odorants in the gas phase are transported differentially through the nasal cavity, then they transfer from the gas phase into the liquid mucus layer close to the olfactory epithelium (OE) and may bind with odor-binding proteins (OBPs). This is the so-called the peri-receptor stage (Pelosi 1996). The next stage involves binding of the odorant to the olfactory receptor (OR) and the subsequent transduction mechanisms. Whereas OR-odorant binding is well researched and the general principles understood (Breer 2008), the peri-receptor stage is a highly dynamic process, which is not so well characterized. In particular, the role of the OBP is unclear and several different hypotheses have been proposed to explain their function. In addition to their odorant-binding property, their high concentrations (0.1–1 mM) (Pelosi 1996) and spatial expression in vivo (Pevsner

et al. 1986) suggest that OBPs play an active role in olfaction, such as in peripheral odor coding (Steinbrecht 1998; Löbel et al. 2002), solubilizing odorants (Pevsner et al. 1990), transferring odorants to and from the ORs (Pevsner et al. 1986; Bignetti et al. 1987; Pevsner and Snyder 1990; Pelosi 1994) or the buffering effect (Taylor et al. 2008).

To elucidate the role of OBPs in the olfaction process, odorant binding to OBP has been studied to determine fundamental parameters such as the dissociation constant (K_d). K_d indicates the potential of the odorant-OBP liquid phase system to react to concentration changes. It is a value that is measured at equilibrium in the liquid phase, using bulk phase conditions and long time periods (Nespoulous et al. 2004). Few publications have considered the overall air–liquid–OBP mass transfer process where several mass transfer processes are linked for example, the gas phase concentration, the air–liquid partition coefficient, diffusion

through the liquid phase, and odorant-OBP binding. Because the odorant concentration in the air phase will cycle between zero (on exhalation) to the measured value (on inspiration), the overall mass transfer is a highly dynamic process, which is unlikely to achieve equilibrium. Previous work (Borysik et al. 2010) used a system that mimicked the overall mass transfer process, and results suggested that the interdependency of the mass transfer processes gave different emphasis to the values obtained from classical kinetic measurements. For instance, the slow off-rates observed in odorant-OBP measurements (using liquid-only phases; Lazar et al. 2002) are not observed in systems that couple the mass transfer processes (Borysik et al. 2010). Other factors like airflow, surface area, and partition coefficients are also involved in overall mass transfer and they may exert significant effects on the odorant-OBP binding through a "push-pull" effect.

The effect of airflow in the nose has been studied by several research groups to understand the relative flows through the convoluted nasal passages and the proportion of air entering the nostrils that actually passes over the OE. Several studies have used computed tomography scans to determine the exact structure of the nasal passages in humans (e.g., Keyhani et al. 1995; Zhao et al. 2004; Croce et al. 2006; Ishikawa et al. 2006, 2009) and in dogs (Craven et al. 2010). These structures have been used with computational fluid dynamic (CFD) techniques to obtain values for linear gas flow at different nasal locations during normal "resting" breathing. For example, the work of Croce et al. (2006) reported a linear velocity of 0.4 m/s in the human olfactory region, a value which agrees closely with the work of Ishikawa et al. (2009) (0.3–0.4 m/s). These papers suggest that under resting breathing conditions, only a small proportion of the airflow passes over the OE on inspiration but more flows over the OE during expiration. In odorant perception terms, this equates to ortho- and retronasal stimulation of the OE. During orthonasal sniffing (when greater volumes of air are inhaled), the flow patterns are shifted so that a greater proportion of the total flow passes the OE during inspiration (Ishikawa et al. 2009). These studies provide accurate values for overall nasal flow and values for the linear velocities near the OE. Deposition of odorants and nanoparticles during orthonasal breathing have been predicted by adding a partition coefficient term to the CFD calculation (Kurtz et al. 2004; Jiang and Zhao 2010), although none of the published papers studied appears to use OBP-specific terms in their calculation of odorant deposition.

Given the continuing uncertainty about the role of OBP in peri-receptor events, an experimental system (Dynamic Biomimetic assay for Odorant Binding System [DyBOBS]) was developed to mimic the conditions found in the human OE and to encompass the mass transfer processes involved (Yabuki et al. 2010). The airflow, the thickness of the liquid layer, the surface area, the odorant concentration, and the concentration of the OBP were all set to values reported in the literature (Yabuki et al. 2010). Because functional human OBP was not available, rat-OBP3 was substituted as it had a close sequence match to human OBP. A known concentration of odorant was passed at known flow rates (volumetric and linear) through a capillary tube coated with a solution of rat-OBP3 and the concentration of odorant leaving the capillary was monitored in real time using gas phase APCI–MS. This simple experimental system was validated (Yabuki et al. 2010) and showed that isobutylthiazole uptake in the presence of OBP was very different compared with a bovine serum albumin (BSA) control, therefore indicating that OBP changed the mass transfer of this compound during the peri-receptor phase.

In the present work, dynamic binding and release of a wider range of compounds (benzaldehyde (BA), 2-methylpyrazine (MP), 2-isobutyl-3-methoxypyrazine (IBMP), 2-isobutylthiazole (IBT), and 2,4,5-trimethylthiazole (TMT)) was studied using DyBOBS. The 5 odorants were used at typical concentrations found in the nasal passages during eating of food (Linforth et al. 2002). The choice of compounds was based on 4 criteria. First, they represent the range of physicochemical properties found in odorants (Table 1). Second, because online APCI-MS could monitor them at the concentrations used. Third, because their binding properties with rat-OBP3 in the liquid phase are known (Löbel et al. 2002; Nespoulous et al. 2004) and fourth, because they exhibit a broad range of dissociation constants with OBP (Table 1). DyBOBS only monitors the odorant concentration in the gas phase and hence measures the net effect of odorant uptake and release. Methods to separate these 2 effects were developed.

We shed some light on various aspects of the initial steps in olfaction under simulated physiological conditions, namely

1. how easily is OBP saturated by an odor ligand?
2. how fast does rat-OBP3 bind and release odor ligands? and
3. how do conditions in the nasal passages (gas flow rate, tidal breathing, and the presence of multiple odorants) affect odorant uptake and release?

For the first part of the investigation, experiments were carried out over long time periods (about 13 min), but for the second part of the investigation, the exposure times were more consistent with physiological conditions.

Experimental procedures

Materials and methods

Odorants (BA, MP, IBMP, IBT, and TMT) >95% purity; Sigma-Aldrich) were dissolved in deionized water at concentrations that delivered gas phase concentrations from 7 to 112 nM (equivalent to 125 and 2500 nl L^{-1} respectively; calculated from the solution concentration using the air–water partition coefficients in Table 1). Portions of odorant

Table 1 Physicochemical and biophysical properties of the 5 odorants used in this study

Odorant	Molecular mass	Air-water partition coefficient[a]	Gas phase [odorant][a] (nM)	Odorant water solubility (mM)	ITC stoichiometry (n) and dissociation constant (K_d)	
					n	$K_d \times 10^{-6}$ (M)
BA	106	1.4×10^{-3}	28.4	51	0.92	687
MP	94	7.1×10^{-5}	17.6	3548	0.81	1.7
IBMP	166	1.5×10^{-3}	16.7	126	0.96	0.47
IBT	141	1.8×10^{-3}	22.3	4.6	0.89	0.067
TMT	127	4.8×10^{-4}	22.3	9.1	0.91	0.026

[a]Determined experimentally using APCI–MS; n = 4 typical variation ± 5%.
The air-water partition coefficient values are the means of 4 replicate measurements, typical variation ± 5%.

solutions (20 mL) were placed in a gas-tight syringe (100 mL; SGE Analytical Science) and allowed to equilibrate, then odorant delivery from the syringe to DyBOBS was achieved using a syringe pump (KD Scientific). The required flow rate was set on the syringe pump and linear velocities were calculated from the capillary diameter (0.53 mm). Humidified odorant-free air was prepared by equilibrating 20 mL of deionized water in a gas-tight syringe.

Rat-OBP3 was over-expressed using *Escherichia coli* M15 cells containing both pREP4 and pQE31, as previously described (Yabuki et al. 2010). BSA (97% purity; Sigma-Aldrich) was used as a control protein. Each protein was dissolved into phosphate-buffered saline (PBS; 137 mM NaCl, 2.7 mM KCl, 10 mM sodium phosphate dibasic, 2 mM potassium phosphate monobasic, pH 7.4) and used for capillary coating using the conditions described before (Yabuki et al. 2010).

Isothermal titration calorimetry

Isothermal titration calorimetry (ITC) measurements were carried out on a MicroCal AutoITC system (MicroCal). Solutions of each odorant were prepared in PBS (300 mM). Titrations were carried out at 21 °C with 30 mM OBP in PBS solution. An initial injection of the odorant solution was followed by 20 more injections of the same solution (14.03 µL each). Blank ligand titrations were also performed to remove the heats of dilution from the odorant/OBP isotherms. The data were analyzed with ORIGIN 7.0 software using the one-site-per-protein-monomer model that is based on the Wiseman Isotherm (Wiseman et al. 1989).

Dynamic odorant-binding assay using APCI-MS

The preparation of thin aqueous OBP and BSA films followed the method of Yabuki et al. (2010). The calculated film thickness for the capillaries used in this study was 1.28 ± 0.07 µm. Five 100-mm capillary sections were taken from a 0.6 m capillary that was internally coated with either a rat-OBP3 PBS solution (0.5–1.25 mM) or a BSA PBS solution (0.5–

1.25 mM). The molar amounts of OBP3 in each capillary were calculated from the concentration of the OBP3 solution and the dimensions of the thin film and ranged from 108 (±7) to 271 (±13) picomoles of OBP3. Capillaries were stored in a sealed glass container at room temperature to minimize dehydration and used for experiments within 6 h of preparation.

Online mass spectrometry

A quadrupole mass spectrometer (Platform II) fitted with a custom-built gas phase APCI interface (Taylor and Linforth 2003) was used. Gas was sampled into the ionization source at 30 mL min^{-1} through a heated (105 °C) deactivated fused-silica tube (1 m × 530 µm inner diameter). Figure 1 shows the system schematically. Odorants were ionized by a 4-kV positive ion corona pin discharge source with a dwell-time of 0.2 s to produce protonated molecular ions. The measured masses were m/z 107 for BA, m/z 95 for MP, m/z 167 for IBMP, m/z 142 for IBT and m/z 128 for TMT. Calibration of the APCI-MS was carried out by introducing an odorant solution (hexane) of known concentration into the APCI-MS at a constant flow rate using a syringe pump (Taylor and Linforth 2003). Masslynx 3.2 software (Micromass) was used to record the ion intensity as a function of time.

Calculation of uptake and release of odorants

The uptake of odorant by OBP was calculated using gas flow rates, gas-phase concentrations, and the time to breakthrough, which was defined as the point when the gas-phase odorant concentration reached half-maximal intensity. The amount of odorant released from the aqueous protein film was determined from the area under the release trace, by monitoring the change in gas phase concentration data with time (area under curve).

Dissociation kinetics

The release curve data from the APCI–MS trace was analyzed using GraphPad Prism 5 (GraphPad Software
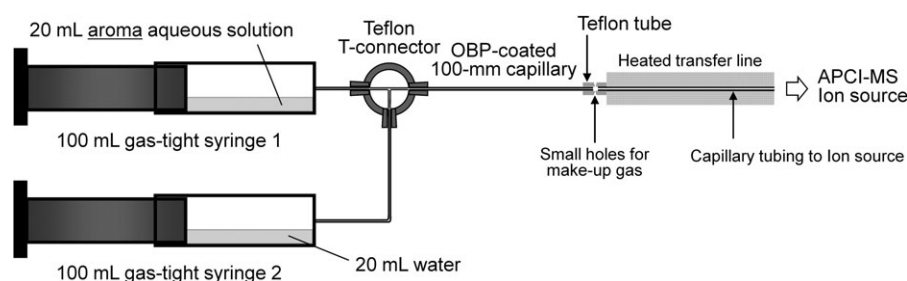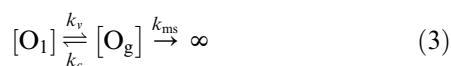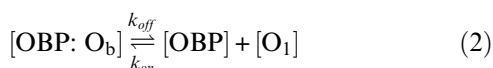
Figure 1 Schematic of the DyBOBS system (Yabuki et al. 2010).

Inc.). The observed off-rate constants for an odorant and rat-OBP3 at a flow rate of 1–20 mL min^{-1} were determined using the first order exponential decay model equation (Equation 1).

$$I_c(m/z, t) = ae^{-kt}, \qquad (1)$$

where I_c (m/z, t), refers to the time-dependent ion current for a protonated molecular ion of a particular mass-to-charge ratio and a and k are the amplitude and first-order rate constants describing the decay in the gas-phase odorant concentration during each experiment, respectively. This assumption was derived from the following 2 equations that describe the mass transfer processes involved (Equations 2 and 3).

$$[OBP: O_b] \underset{k_{on}}{\overset{k_{off}}{\rightleftharpoons}} [OBP] + [O_1] \qquad (2)$$

$$[O_1] \underset{k_c}{\overset{k_v}{\rightleftharpoons}} [O_g] \overset{k_{ms}}{\rightarrow} \infty \qquad (3)$$

where k_{off}, k_{on}, k_v, k_c, and k_{ms} are the respective microscopic rate constants for dissociation, association, odorant release, odorant deposition, and APCI–MS consumption. [OBP:O$_b$], [OBP], [O$_1$], [O$_g$] are the molar concentrations of the odorant-OBP3 complex, free OBP3, free aqueous odorant, and gas-phase odorant respectively, and ∞ is a sink to the mass spectrometer. Because the OBP and BSA films used in this study were thin (around 1 μm), odorant mass transfer in the liquid phase will be by diffusion and will be of the order of 1 ms (Taylor et al. 2008). Previous work indicated that changes in the gas phase odorant concentration should be followed by a change in the liquid phase odorant concentration within a period of 100–200 ms (Taylor et al. 2008). Thus, when the APCI–MS sampling rate, k_{ms} is faster than the time needed for the gas phase odorant to reestablish the steady state, time-dependent changes in free aqueous odorant concentration can be inferred from the changes in gas-phase odorant concentration in the capillary.

Results

Selection of odorants

Air–water partition coefficients, water solubility values, and ITC results (n, binding stoichiometry; K_d, dissociation constant) for the 5 odorants used in this study are summarized in Table 1. Odorant concentrations are expressed either in molar or in volume terms depending on context as partition and stoichiometry are expressed as a molar ratios, wheras release is expressed in volumes. The odorants exhibited a wide range of binding affinities for rat-OBP3 from 0.067×10^{-6} M to 687×10^{-6} M (K_d) and a range of water solubilities. Air–water partition coefficients were experimentally measured on the APCI–MS (Marin et al. 1999) as values in the literature varied considerably for some compounds. Water solubility values were estimated using an on-line software program (ALOGPS 2.1, http://www.vcclab.org). ITC experiments were carried out to determine the dissociation constants (K_d values) of the odorants used and to confirm the integrity of the protein. The K_d value obtained for IBT (0.067×10^{-6} M) was 7 times smaller than previously reported in the literature (0.47×10^{-6} M) (Löbel et al. 2001). The inability of BSA, a control protein, to bind the 5 tested odorants was also confirmed using ITC (data not shown).

Binding and release traces using APCI–MS

To compare the effect of OBP concentration on odorant uptake, each odorant was introduced independently into the capillaries coated with a thin film of rat-OBP3 in PBS solution (0.5, 0.75, 1, and 1.25 mM). Control experiments used capillaries coated with the same concentrations of BSA to monitor the effect of dissolution of odorants in the aqueous phase and to assess any nonspecific binding by the BSA protein.

To assess binding capability, the experiment was run over long time periods to saturate the OBP with odorant and determine binding stoichiometry. Figure 2 shows typical APCI–MS traces of gas-phase binding and release of BA from BSA and OBP3 at different concentrations. BA in air (28.4 nM ≈ 640 ppbv) was passed through the OBP-coated capillary for 13 min at 1 mL min^{-1}, then substituted by odorant-free air from another syringe (same flow rate) up
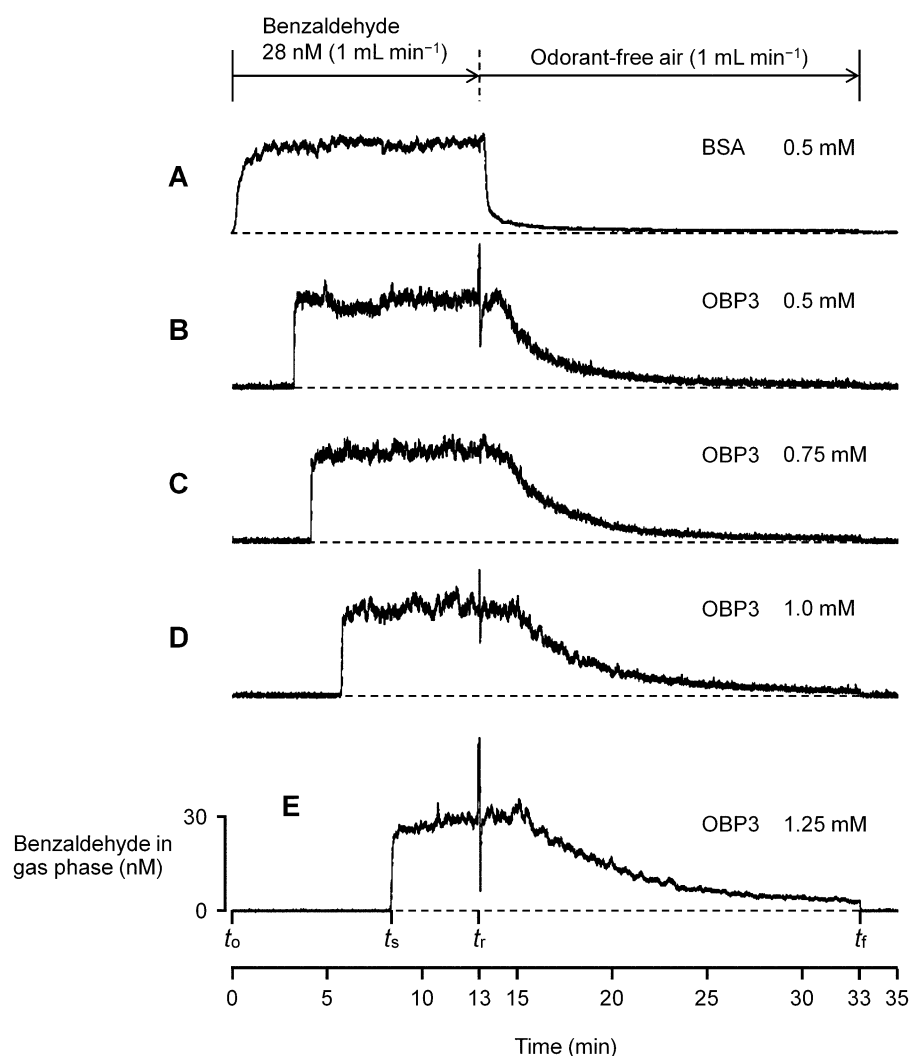
Figure 2 Typical APCI-MS traces from capillaries coated with 0.5 mM BSA **(A)** or with different concentrations of rat-OBP3 **(B–E)** (t_0 = introduction of odorant-containing air, t_s = time when the capillary become saturated with the odorant, t_r = introduction of odorant-free air, t_f = time when the odorant-free air delivery terminates). BA (28.4 nM) was introduced into the protein-coated capillaries from time 0 to 13 min at 1 mL min^{-1}. Odorant-free air was introduced into the capillaries for 20 min (from 13 to 33 min) at the same flow rate, and the gas delivery was then turned off at 33 min. The gas-phase BA concentration was monitored (*m/z* 107) and sub-figures A through E are all on the same *y* axis scale.

to 35 min. The on-line APCI-MS monitored the concentration of odorant in the gas phase exiting the capillary and the trace can be interpreted as follows. No signal on the trace denoted that the odorant was being completely taken up by the protein film in the capillary while the appearance of odorant signal denoted breakthrough of odorant (in the period up to 13 min) and release of odorant (after 13 min).

Odorant uptake by 0.5 mM BSA was marginal (Figure 2A) as the introduction of BA into the capillary resulted in a rapid rise in the gas-phase odorant concentration, up to the signal level found when a 28.4 nM BA concentration was analyzed directly by the APCI–MS. The rapid rise in APCI signal around t_0 showed that BA binding to BSA was insignificant. The introduction of odorant-free air at 13 min (t_r) caused a sharp decline in the gas-phase odorant concentration to

baseline values within 0.5 min. Traces obtained using 0.75–1.25 mM BSA concentrations showed very similar patterns to Figure 2A (data not shown).

In contrast, when BA was introduced into rat-OBP3–coated capillaries, the shapes of the traces were different compared with the BSA trace. Initially, the gas-phase odorant signal remained at baseline level for 3.3 min for the 0.5 mM OBP3 capillary (Figure 2B). This was followed by a sudden increase in the gas-phase odorant concentration. The time (t_s) for BA to break through to the end of the capillary (and achieve a signal level equivalent to 28.4 nM) was delayed as the concentration of OBP3 increased (Figure 2B–E). When the flow was switched to odorant-free air, a gradual decrease in the gas-phase odorant concentration occurred. As OBP3 concentrations increased, the amount of odorant released (as well as the time taken for release) also increased.

The APCI–MS traces for the 4 other odorants showed similar patterns, but there were differences in the binding and release behaviors, which are analyzed in the following sections.

Odorant uptake by OBP

The amount of OBP on each capillary was calculated (pico-moles) and the uptake of odorant by the protein films was calculated from the APCI traces between the t_0 and t_s times since the gas flow rate and odorant concentration in the gas phase were known. These calculations were carried out for all 5 odorants tested (see Table 1) and at each OBP3 concentration (0.5–1.25 mM). Stoichiometry values (Table 2) were calculated as the molar ratio between the amount of odorant taken up, divided by the OBP content in a capillary. Overall, there was a small (but insignificant) trend of higher values at low OBP concentrations. Most stoichiometry values were around 1 with only MP showing a value >1. The behavior of MP can be rationalized as it is much more soluble in water than the other odorants tested and its K_{aw} favors the aqueous phase (Table 1). Therefore, over the time to breakthrough, the MP is taken up by both the OBP and the aqueous film and the contribution from the latter may over-estimate the stoichiometry value. By assuming 1:1 MP:OBP stoichiometry, the concentration of MP in the purely aqueous phase was 75 μM. If we assume that equilibrium between the gas and liquid phases is achieved in the condition that DyBOBS was operated in, we can compare the expected liquid phase concentration (248 μM) against the observed value (75 μM). This comparison acts as a sense check in that the liquid phase concentration cannot be more than the equilibrium value (248 μM). Although these calculations are subject to error amplification (as any error in the K_{aw} value exerts a large effect through the calculation process), the values support the hypothesis that the physicochemical properties of MP can explain the fact that the stoichiometry value calculated in this system is an over-estimate. Inspection of the physico-chemical data for the other compounds shows that TMT is the only other compound with a K_{aw} value that might en-courage water solubility over OBP binding. However, the

Table 2 Stoichiometry of odorant binding to rat-OBP3 at different OBP concentrations in the DyBOBS system

OBP concentration (mM)	BA	MP	IBMP	IBT	TMT
0.5	1.06	1.35	0.97	0.76	1.07
0.75	0.78	1.08	0.97	0.94	0.86
1	0.86	1.06	0.96	0.77	0.93
1.25	0.80	1.00	0.92	0.82	0.82
Mean values	0.87	1.12	0.96	0.83	0.92

Values are the mean of 5 replicates.

water solubility of TMT is much lower than MP and this may affect the relative amounts of TMT in the aqueous and bound forms. A simple calculation shows that there is the potential to significantly concentrate odorants in the OBP film. If the gas-phase odorant concentrations are around 20 nM and the OBP concentration is 1 mM, then a 50 000 fold concentration is possible.
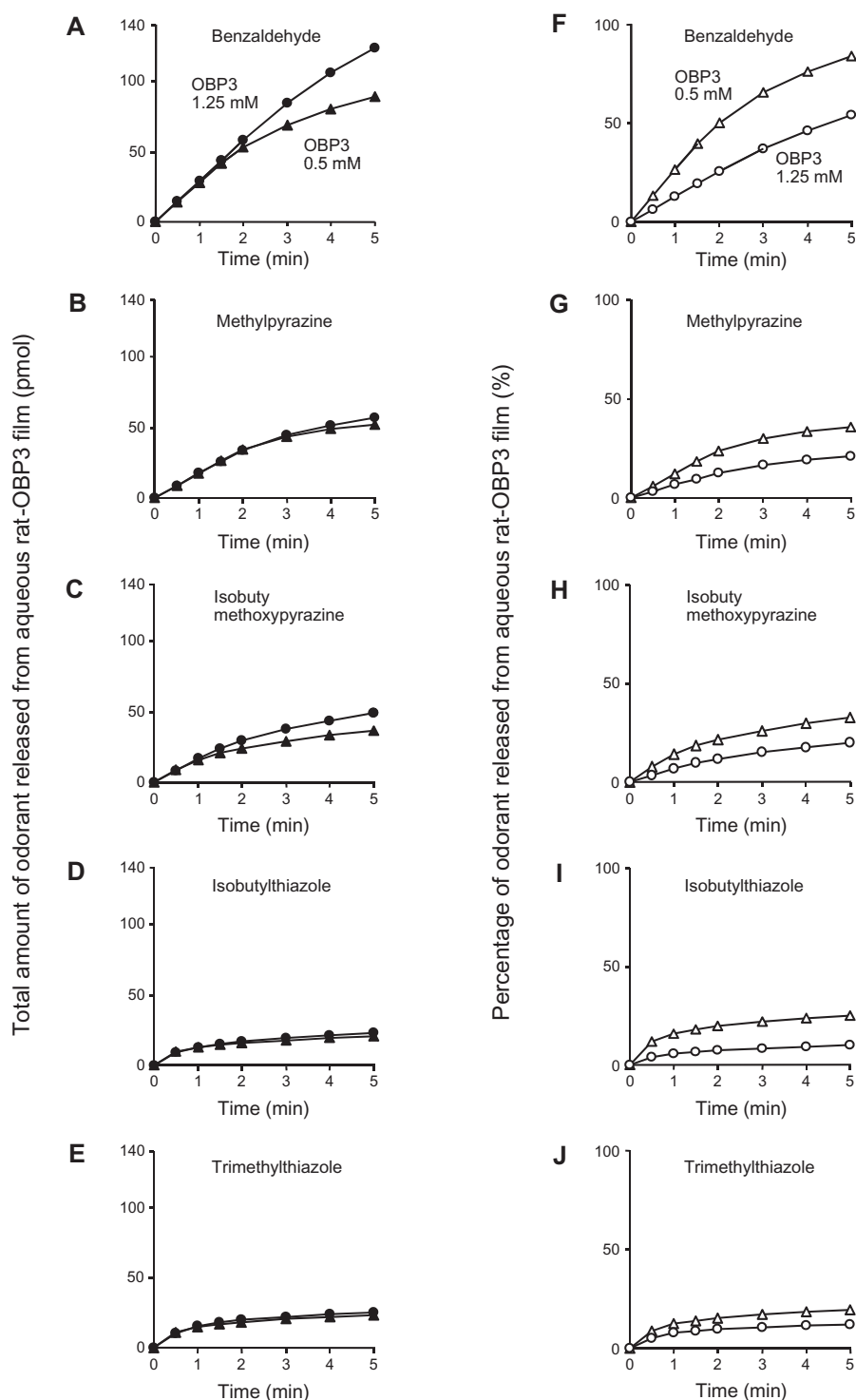
Odorant release from OBP

To investigate the dynamics of odorant release from rat-OBP3, the time-dependent changes for the amount of the 5 selected odorants released were calculated from the data used for the calculation of uptake amount. Examples of release traces for BA are shown in Figure 2B–E (from 13 to 33 min). Figure 3A–E shows the total amount of each odorant that was released from the capillary coated with 0.5 mM OBP3 (black triangles) or 1.25 mM OBP3 (black circles). The starting points of the release curves (0 min) in Figure 3A–E correspond to the injection time of odorant-free air as shown at 13 min (t_r) for BA in Figure 2B–E. There was an upward trend in the release amount with an increase in the dissociation constant of the odorant tested (see Table 1), suggesting that the differences in the release amounts between the odorants were attributable to the affinity of the odorant for rat-OBP3. For BA and IBMP, the release amounts from the capillaries coated with a higher (1.25 mM) concentration of OBP3 were greater than those from capillaries with a lower (0.5 mM) concentration of OBP3 film.

Figure 3F–J shows the percentage of released odorant, which is based on the amount of odorant taken up before the introduction of odorant-free air for 0.5 mM rat-OBP3 (open triangles) or 1.25 mM rat-OBP3 (open circles). Over-all, at the same OBP concentration, the proportion of the amount released, to the uptake amount, depended on the affinity for OBP3. For example, release of BA, which has the weakest affinity for rat-OBP3 among tested odorants (Table 1), was significant, reaching 84% at the 0.5 mM concentration level (Figure 3F). Full release of BA took about 9 min from the 0.5 mM OBP3 film. At 1.25 mM OBP3, approximately 54% of the BA odorant molecules were re-leased over 5 min. Release of MP and IBMP, which have intermediate affinities for rat-OBP3 of the selected 5 odor-ants, was moderate, and both exhibited similar release curves (Figure 3G,H). The release of MP at 5 min post-introduction of odorant-free air reached 36% and 21% at 0.5 mM and 1.25 mM, respectively. The release of IBT and TMT, which have small dissociation constants, was insignificant (Figure 3I,J). The release amounts of TMT at 5 min were 19% and 12% at 0.5 and 1.25 mM, respectively (Figure 3I). MP, IBMP, IBT, and TMT were not fully released in the 20 min introduction of odorant-free air. The proportion of odorant molecules released by odorant-free air decreased as the OBP3 concentration increased.

Figure 3 Time-dependent curves for the release amount (pmol) of the 5 selected odorants from 0.5 mM aqueous rat-OBP3 film (black triangles) and from 1.25 mM aqueous rat-OBP3 film (black circles) **(A–E)**. Time-dependent curves for the percentage of the 5 selected odorants released from 0.5 mM aqueous rat-OBP3 film (open triangles) and from 1.25 mM aqueous rat-OBP3 film (open circles) **(F–J)**. Each odorant (at the concentration in Table 1) was introduced at 1 mL min^{-1} into the capillary.
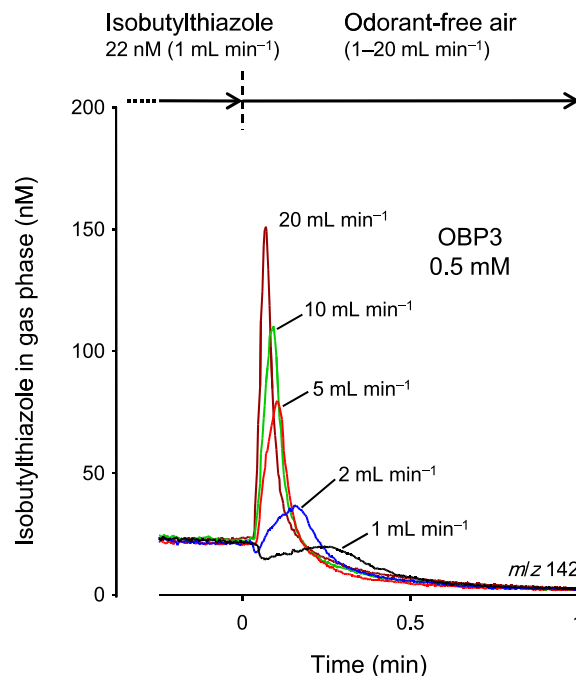
Effect of airflow rate on odorant release

To investigate the effect of airflow rate on odorant release, OBP was fully loaded with odorant, then odorant-free air was introduced at different flow rates. The changes in the release traces for BA and IBT, which were the weakest and strongest binding odorants, respectively (Table 1), are
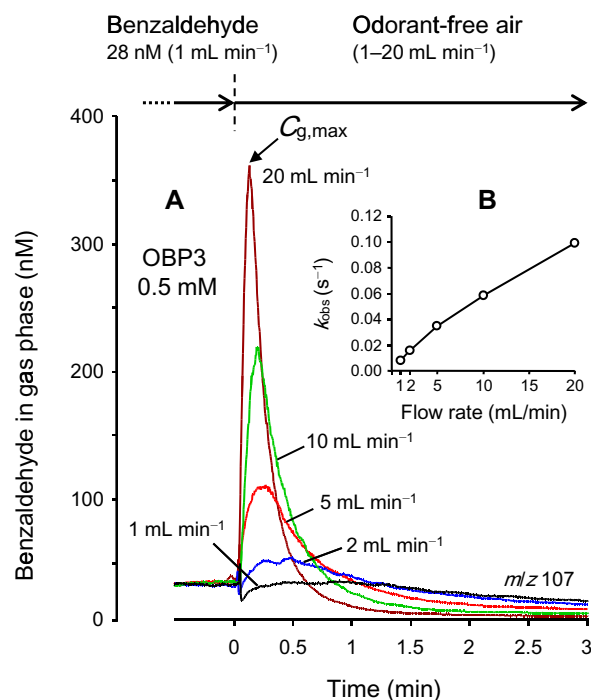
Figure 4 Examples of the effect of airflow rate on odorant release for BA **(A)**. BA (at the concentration in Table 1) was introduced into the rat-OBP3 capillary (0.5 mM OBP3) at 1 mL min^{-1} until the capillary was fully saturated with the odorant. Different flow rates (1, 2, 5, 10, or 20 mL min^{-1}) of odorant-free air were then introduced into the system. Changes in the observed off rates of BA OBP3 complex at different flow rates **(B)**. The k_{obs} was determined by fitting the release curves starting from the highest headspace concentration ($C_{g,max}$) to the first-order exponential decay model equation.

Figure 5 Examples of the effect of airflow rate on odorant release for IBT. IBT (at the listed concentration in Table 1) and odorant-free air were sequentially introduced into the rat-OBP3 capillary (0.5 mM OBP3) in the same manner for BA in Figure 4.

Table 3 Hydrodynamic parameters of odorant-free air used for BA and IBT dissociation kinetics study and the theoretical evacuation time of the capillary

| Flow rate (mL/min)	Linear velocity (cm/s)	Reynolds number (Re dimensionless)	Theoretical evacuation time (ms)
1	8	3	1 310
2	15	5	655
5	38	13	262
10	76	26	131
20	153	51	66

For calculation, the averaged thickness of aqueous OBP film (1.28 μm), which was determined from the results of 20 independently performed coating experiments (the 5 odorants × the 4 concentrations), was used.

shown in Figures 4 and 5. Each odorant was introduced into the OBP3-coated capillaries (0.5 mM) at 1 mL min^{-1} until the system was fully saturated with odorants (6 min). Once saturation was reached, odorant-free air was introduced at a flow rate of 1–20 mL min^{-1} (linear velocity of 8–153 cm s^{-1}) (Table 3). The rate of BA release was strongly affected by the flow rate of odorant-free air (Figure 4A). At 20 mL min^{-1}, the release rate reached a maximum value of about 13 times faster than the value obtained at 1 mL min^{-1} and rapid odorant release continued for about 0.5 min. Almost all the BA molecules were released from the aqueous OBP film within 1.5 min. When lower flow rates of the odorant-free air were used, values for the maximum release rate decreased, and the time-dependent changes in the release rate became gradual. The decay curve of the gas-phase BA concentration starting from their highest concentration ($C_{g,max}$) fitted well ($R^2 > 0.99$) to a single exponential equation (Equation 1). The observed off-rate constants calculated increased from 0.01 s^{-1} at 1 mL min^{-1} to 0.1 s^{-1} at 20 mL min^{-1} (Figure 4B). Although the initial rate of release was affected by the flow rate of odorant-free air, the change in the release curve for IBT was moderate (Figure 5) in comparison to the changes observed for BA. For example, as the flow rate of odorant-free air increased to 20 mL min^{-1}, the maximum

IBT release rate increased to 7 times that of the value obtained at 1 mL min^{-1}; however, a rapid decrease in the release rate was observed within 0.5 min of odorant-free air introduction, and the gas-phase odorant concentration decreased.

Cycling airflows to mimic nasal tidal flow

To study how fast rat-OBP3 binds and releases odor ligands and to test the reversibility of odorant binding, BA, the weakest-binding odorant was chosen as the model odorant because rapid release from the OBP-odorant complex was observed in previous experiments (Figures 3A and 4A). BA (125 ppbv ≈ 7 nM in air) was introduced into aqueous 0.5 mM BSA- or
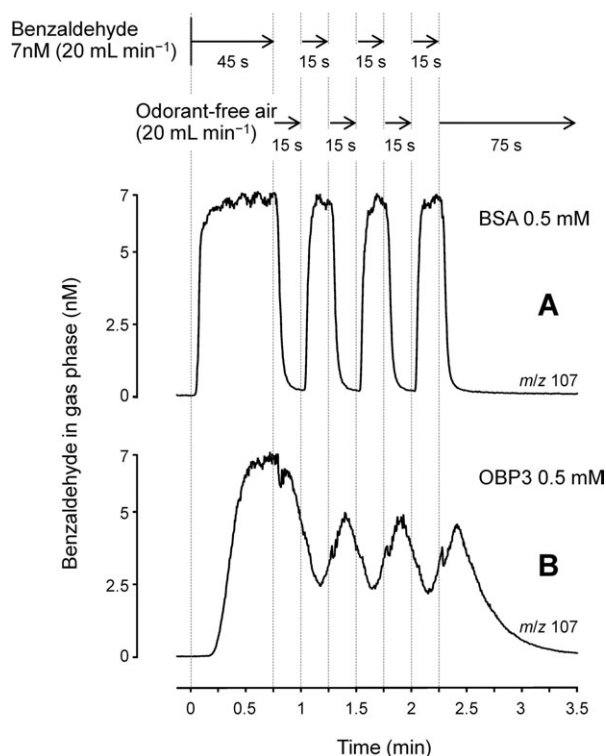
Figure 6 BA traces when introduced in cycles into a BSA capillary **(A)** or rat-OBP3 capillary **(B)** to mimic the nasal tidal flow and to study the uptake and release kinetics of odorant binding to OBP under physiologically relevant gas flow conditions. BA gas (7 nM ≈ 160 ppbv) was introduced at 20 mL min^{-1} into the protein-coated capillaries (0.5 mM BSA or OBP3) from 0 to 0.75 min (45 s). Odorant-free air and BA were introduced in turn into the capillary at the same flow rate 3 times, each for 0.25 min (15 s). Finally, odorant-free air was introduced into the system for 1.25 min (75 s).

OBP3-coated capillaries at 20 mL min^{-1} for 45 s. Subsequently, 15 s of odorant-free air was followed by 15 s of BA in air and the cycle repeated 3 times (each 15 s). Finally, odorant-free air was introduced for 75 s (Figure 6A,B). In the BA trace from the BSA-coated capillary, rapid increases and decreases in the gas-phase concentration were observed as the flow changed in each cycle (Figure 6A). Full saturation of the rat-OBP3 capillary (0.5 mM) with BA was obtained at about 40 s (Figure 6B). After replacing the BA gas with odorant-free air, a gradual decrease in the gas-phase BA concentration by about 4.5 nM was observed. When the second BA flow was introduced, a decline in the gas-phase BA concentration continued, ultimately reaching about 2.5 nM. The OBP3-film became saturated again and the gas-phase BA concentration started to increase. When odorant-free air was reintroduced, the gas-phase BA concentration increased to about 4.8 nM. Increases and decreases in BA gas-phase concentrations repeatedly occurred during subsequent cycles. When the final volume of odorant-free air (75 s) was introduced, the gas-phase concentration of BA reached approximately 4.5 nM then decreased gradually and approached the base line.

Competitive binding

To investigate competitive odorant uptake and release by rat-OBP3, 2 odorants were first introduced into the capillary sequentially. IBMP and IBT (at the concentrations in Table 1) were chosen because these 2 odorants have different binding affinities for rat-OBP3 (medium and high, respectively; Table 1). Figure 7A shows the gas-phase IBMP trace when IBMP and odorant-free air were sequentially introduced into the OBP3 capillary (0.75 mM) at 3 mL min^{-1} over three 5 min cycles. Odorant uptake and release by OBP3 occurred on a regular, periodic basis which followed the cycle of IBMP and odorant-free air introduction, although with a time lag. Release of IBMP during the 5 min cycle with clean air was not quantitative as the time for the OBP to become fully loaded in the second and third cycles was shorter, than the first cycle. Figure 7B shows the results when the experiment was repeated but with IBT in place of the clean airflow. IBT has a lower K_d (0.067×10^{-6} M) than IBMP and should bind more strongly to OBP. The competitive effect can be clearly seen at 6 min on the trace in Figure 7B where IBMP is displaced from the OBP when IBT is introduced into the gas phase. A similar but smaller effect is seen in cycles 2 and 3 (16 and 26 min). There is an effect on IBMP uptake in cycles 2 and 3 presumably because IBT is occupying the OBP-binding sites and IBMP can only partially displace some of the IBT molecules. In cycle 2 of the IBT, the OBP becomes fully loaded with IBT in a shorter time than in cycle 1, showing that limited release/displacement occurred in the cycle time between 11 and 16 min.

Figure 7C shows the situation when IBMP and IBT are introduced simultaneously. Traces a–e show how the concentration of IBT affects the release of IBMP with time. IBMP concentration was held at 190 ppbv (≈8.4 nM), whereas IBT levels were 0, 250, 500, 1000, or 2500 ppbv (0, 11, 22, 45, or 112 nM, respectively). Rat-OBP3 concentration was 0.75 mM and total flow rate was 6 mL min^{-1}. In the absence of IBT, the aqueous OBP3 layer took about 2.7 min to become saturated with IBMP (Figure 7C—e); however, in the presence of IBT, the amount of IBMP uptake became smaller. With the same concentration of IBT, the aqueous OBP3 layer was saturated within 1.4 min and the uptake amount of IBMP was about half of the original amount. At a low concentration of IBT (250 ppbv ≈ 11 nM), a steady release rate was observed (Figure 7C-d); whereas at higher concentrations of IBT (500–2500 ppbv), the IBMP peak shape became sharper as the IBT concentration increased (Figure 7C—a to c). The decay curve of the gas-phase IBMP concentration starting from their highest concentration fitted well to a single exponential equation (Equation 1; $R^2 > 0.97$), and the values were in the range from 4 to 15 min^{-1}. Corresponding half-life values of IBMP–OBP3 complex were between 3 and 10 s.
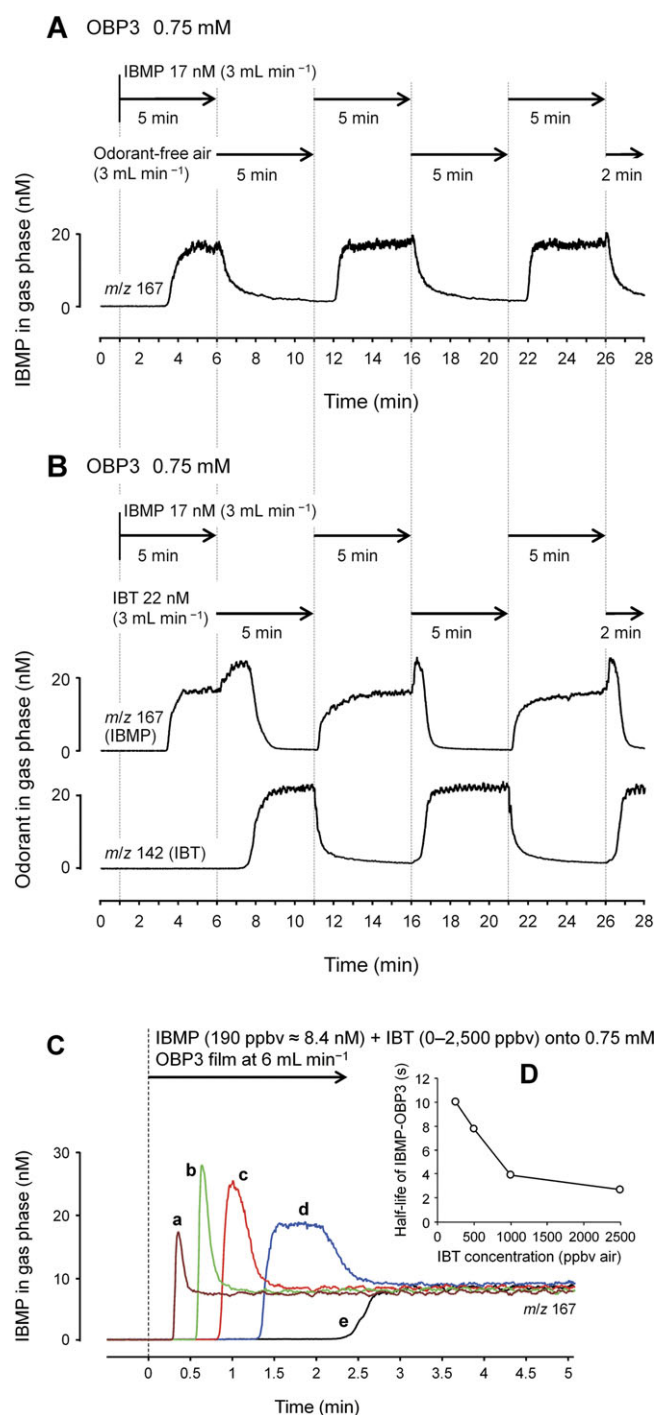
Figure 7 Differences in IBMP traces (*m/z* 167) in the absence and presence of IBT (A and B). IBMP (at the concentration in Table 1) was introduced into the rat-OBP3 capillary (0.75 mM) at 3 mL min⁻¹. After the OBP3 capillary was saturated with odorant, odorless air **(A)** or IBT at the concentration in Table 1 **(B)** was introduced at the same flow rate and for the same duration. A pair of gases was presented three times, one after the other. Differences in IBMP traces with different concentrations of IBT introduced into the capillary simultaneously **(C)**. IBMP (190 ppbv ≈ 8.4 nM) and IBT (0–2500 ppbv air) were introduced into the rat-OBP3 capillary (0.75 mM) at 3 mL min⁻¹. The chromatogram **a–e** show IBMP traces in the presence of decreasing concentrations of IBT (**a**, IBT 2 500 ppbv; **b**, 1 000 ppbv; **c**, 500 ppbv; **d**, 250

Discussion

The DyBOBS system measures odorant binding to OBP indirectly that is, by monitoring the change in odorant concentration in the outflow of the system (Figure 1). Previous work (Yabuki et al. 2010) has established the validity of this indirect approach through a series of control experiments, which studied potential confounding factors. The results showed that there was no significant binding to components of the DyBOBS system (e.g., the capillary itself) and that nonspecific binding to proteins like BSA was insignificant. Aqueous solubility of the odorants is known (Table 1) and this contribution can be calculated (see earlier discussion in Odorant uptake by OBP).

The purpose of the first experiments was to investigate the uptake and release behavior of 5 odorants under simulated OE conditions. A comparison of stoichiometry values obtained by ITC and DyBOBS shows good agreement (Tables 1 and 2), with only the values for MP (ITC 0.81; DyBOBS 1.12) showing disparity. Given the discussion in previous sections about the high solubility of MP in water and the fact that the ITC results were corrected for dissolution of odorants in water, this is not really surprising. The other key outcome of the stoichiometry data is that with near 1:1 binding, the potential concentration factor for odorants can be up to 50 000 times (based on 1 mM OBP and an odorant gas phase concentration of 20 nM). Another outcome is to estimate the odorant flux in the system. At 1 mL min⁻¹ flow and a concentration of 20 nM, about 20 pmol of odorant min⁻¹ were delivered and taken up by the OBP layer as no odorants exited the capillary and were detected by the APCI-MS during this time. This suggests that the speed of odorant mass transfer from the gas to the liquid phase in the model system was faster than the rate of odorant delivery in the gas phase. Assuming the probability for an odorant to contact the OR can be estimated as the concentration of the odorant in the OE multiplied by the residence time of the odorant, the concentrating effect could potentially increase the chance for odorants to contact the OR. Firestein et al. (1993) have reported that the ORs are not only responsive to the odorant concentration, but that they also sense the accumulated effects of the stimulus over time. In such a situation, OBPs could potentially enhance the output signal from the receptor cells. Pevsner et al. (1990) studied the odorant release kinetics of bovine OBP utilizing the infinite dilution technique for blocking the reassociation of dissociated odorants and bovine OBP. They reported that the dissociation of IBMP was very slow with negligible dissociation after 1 h. In the present study, the dissociation of MP, IBMP, IBT, and TMT were slow in comparison to BA, but the percentage of the released odorants were between 10% and 36% over

ppbv and **e**, 0 ppbv). The half-life values of IBMP–OBP3 complex were calculated by fitting the release curves starting from the highest headspace concentration to the first-order exponential decay model equation **(D)**.

5 min of odorant-free air introduction. It is likely, in DyBOBS, that the release occurs in much shorter time periods under the conditions where the reassociation of IBMP and rat-OBP3 are blocked.

To study the dynamic odorant binding to OBPs, model systems need to take into account the OE airflow profile in vivo. Keyhani et al. (1997) have employed an anatomically correct 3D finite model, and their computational airflow simulations have shown that the average olfactory air speed was about 0.90 m s^{-1} for resting breathing. Ishikawa et al. (2009) recently investigated human nasal airflows using a CFD method and compared the inspiratory phase, expiratory phase, and sniffing flow patterns at different nasal locations. They reported that the velocity in the region of the OE during normal respiration was about 0.4 m s^{-1}. The linear velocities in the DyBOBS system were between 0.08 m s^{-1} (a flow rate of 1 mL min^{-1} [Reynolds number 3]) and 1.53 m s^{-1} (20 mL min^{-1} [Reynolds number 51]) to fully encompass the average olfactory air speed found by Keyhani et al and Ishikawa et al (Table 3).

In our model system, the residence time and rate of odorant release were strongly dependent on the odorant affinities for the protein and the amount of OBP3 (Figure 3F–J). When odorant-free air was introduced at a flow rate of 1–20 mL min^{-1} (a velocity of 0.08–1.53 m s^{-1}) into the system after the aqueous OBP3 layer was fully saturated with BA, the release of BA, a weakly binding odor ligand, was greatly affected by the airflow rate. Under high flow conditions, odorant release was accelerated (Figure 4). The dramatic changes in release can be explained by reference to basic chromatography principles. Simply speaking, at high flow rates, a molecule that is released into the gas phase is swept down the column and has fewer chances of rebinding with OBP in the liquid phase, so exits the capillary faster. At a flow rate of 20 mL min^{-1}, the theoretical evacuation time of the capillary is calculated to be 70 ms (Table 3). Therefore, the evacuation rate constant, k_{ms} should be greater than the time needed for achieving equilibrium between the gas and liquid phases (k_v and k_c), meaning that the observed time-dependent changes in gas-phase odorant concentration directly relates to the change in free odorant concentration in the liquid phase. The results suggest that the gas flow rate (velocity) significantly affects the odorant residence time in the OE and that high airflow rates may contribute to the clearance of odorants so that OBPs can readily bind air-borne odorants within breathing airstreams.

To test how fast OBPs bind and release odorants, BA and odorant-free air were alternately introduced into the OBP3-coated capillary at short time intervals (Figure 6). When odorant-free air was introduced into the system after the aqueous rat-OBP3 layer was first saturated with BA, an initial decrease in the gas-phase concentration was observed (Figure 6B). As shown in the BSA data (Figure 6A), the gas-phase odorant took 10 s to dissipate once the syringe pump

controlling introduction of the gaseous BA was turned off and the syringe pump controlling introduction of the odorant-free air was turned on. This is because a gas-tight syringe that works by a pressure-driven mechanism experiences lag time before the syringe actually stops or starts delivering either the gas-phase odorant or the clean odorant-free air into the OBP3 capillary. After an initial drop, a small peak can be seen in gas-phase odorant concentration (Figure 6B), indicating that there may have actually been a release of odorant by the OBP, and this was masked by the excess odorant overflowing from the gas-tight syringe containing the BA solution. When odorant-free air was introduced into the system, in which the aqueous rat-OBP3 film was not saturated with BA, as the second or the third introduction, small peaks due to the overflow of the odorant, followed by an increase in the gas-phase odorant concentration, were observed. The gas-phase BA concentration started to increase prior to the introduction of odorant-free air in all cases after the initial BA injection, indicating the OBP3-film became saturated again. It is unclear if partitioning between the 2 phases at the OE occurs in vivo as often as in the model system that utilized a relatively long (100 mm) but narrow capillary tubing (internal volume ∼ 22 μL). Therefore, although complete odorant release was not observed in the 15-s intervals used in this study (Figure 6A,B), it seems possible that odorants with binding affinities for rat-OBP3 much weaker than BA are released at normal breath cycles, which occur at 4–5 s for humans (Keyhani et al. 1995) and around 0.4 s for rats (Walker et al. 1997), to prepare for the next odor stimulus.

To investigate uptake and release properties in the presence of a competitive binder, IBMP and IBT, which have different affinities for rat-OBP3 (see Table 1), were introduced sequentially into the OBP capillary (Figure 7B). Whereas continuous IBMP uptake and release occurred repeatedly in the absence of IBT (Figure 7A), which is a tight-binding odor ligand, odorant uptake for IBMP was limited in the presence of IBT. This result suggests that when a tight-binding odor ligand is introduced, displacement occurs easily; conversely, when OBPs bind to a strong-binding odor ligand, uptake of a weak-binding odor ligand is limited. When IBMP and IBT were introduced simultaneously into the rat-OBP3 capillary, the IBMP uptake amount was altered (Figure 7C). Moreover, the residence time of IBMP became shorter, and the rate of IBMP release rate became faster. The release of IBMP from aqueous OBP3 film occurred within very short time periods (3–10 s). The half-life value for IBMP-OBP3 complex was as short as 3 s when 2500 ppbv (112 nM) concentration of IBT was introduced; the value is 2 orders of magnitude faster than the literature (Pevsner et al. 1990) has previously suggested. These results indicate that multiple binding and release from OBPs occur in vivo, where diverse odorants exist, and occur simultaneously with release rate constants (k_{off}) that are actually relevant to detecting odors. As rat-OBP3 exhibits typical OBP characteristics (Löbel et al.

2002, 2001), it is likely that vertebrate OBPs generally display similar results to those shown in this study.

Conclusion

What is currently missing from our understanding of olfactory perception is a detailed knowledge of the mass transfer mechanisms that occur when odorants in the gas phase pass over the OE and odorants transfer from the gas phase to the liquid phase and finally to the ORs. The observations presented in this paper provide fundamental information on the first peri-receptor events in olfaction and contributes to the current knowledge concerning the role of OBPs. The investigation could be further continued by including a secondary phase to study the transfer of odorants from OBPs to ORs. The lack of a functional stable human OBP is a current limitation. The effects of various OBP subtypes also need to be studied. The dynamic release and displacement of odor ligands and the mass transfer of dissociated odorants between the gas and liquid phases within the time scale relevant to odor detection suggest that dissociated odorants could be involved in peripheral event(s) in olfaction. Because rat-OBP3 has been shown to display typical OBP characteristics, the data indicate that vertebrate OBPs may play a role in increasing the mucus-phase odorant concentration, which could potentially enhance the frequency and duration of odorant access to the olfactory neurons.

The transport of odorants through the DyBOBS system is clearly mediated by the presence of OBP: an apparent retardation in odorant release is seen quite clearly (Figure 2). The degree to which each odorant is affected differs, and this therefore needs to be explained in terms of the kinetics of transfer from the gas phase, how these kinetics are affected by OBP3 in the solution phase, and the intrinsic binding affinity of OBP3 for these odorants. The experiments provide access to 2 parameters:

A. The intrinsic solution-based affinity of OBP3 for a particular odorant, as determined by isothermal titration calorimetry and
B. The time-dependent concentration of the odorant in the gas phase as it emerges from the DyBOBS system.

Our ligands can be broadly categorized into 4 classes:

1. Hydrophilic with a high affinity (low K_d) for OBP3.
2. Hydrophobic with a high affinity (low K_d) for OBP3.
3. Hydrophilic with a low affinity (high K_d) for OBP3.
4. Hydrophobic with a low affinity (high K_d) for OBP3.

Each of these will show a distinct behavior in the DyBOBS system in the presence of OBP3. In the absence of OBP3, the odorant partition between the gas and the liquid phase will depend upon the rate of condensation of the odorant into the liquid phase, the rate of volatilization out of the liquid phase, and the flow rate of carrier gas through the system. In the presence of OBP3 there are further processes. We assume that OBP3 cannot directly obtain odorants from the gas phase and therefore interacts only with those in the solution phase. Hence, if a hydrophilic ligand that binds tightly to OBP3 is introduced into DyBOBS, then there is a strong effect of retardation, and hence a slower rate of release is observed. If the ligand is hydrophobic, a rate of release is still seen, but its magnitude is much less as there will be less soluble ligand available. If a ligand does not bind tightly to OBP3, then the rate of release will more closely depend on the off-rate of the ligand/protein complex.

Acknowledgements

References

Bignetti E, Damiani G, Denegri P, Ramoni R, Avanzini F, Ferrari G, Rossi GL. 1987. Specificity of an immunoaffinity column for odorant-binding protein from bovine nasal-mucosa. Chem Senses. 12:601–608.

Borysik AJ, Briand L, Taylor AJ, Scott DJ. 2010. Rapid odorant release in mammalian odour binding proteins facilitates their temporal coupling to odorant signals. J Mol Biol. 404:372–380.

Breer H. 2008. The sense of smell—reception of flavors. Ann N Y Acad Sci. 1126:1–6.

Craven BA, Paterson EG, Settles GS. 2010. The fluid dynamics of canine olfaction: unique nasal airflow patterns as an explanation of macrosmia. J R Soc Interface. 7:933–943.

Croce C, Fodil R, Durand M, Sbirlea-Apiou G, Caillibotte G, Papon JF, Blondeau JR, Coste A, Isabey D, Louis B. 2006. In vitro experiments and numerical simulations of airflow in realistic nasal airway geometry. Ann Biomed Eng. 34:997–1007.

Firestein S, Picco C, Menini A. 1993. The relation between stimulus and response in olfactory receptor-cells of the tiger salamander. J Physiol. 468:1–10.

Ishikawa S, Nakayama T, Watanabe M, Matsuzawa T. 2006. Visualization of flow resistance in physiological nasal respiration: analysis of velocity and vorticities using numerical simulation. Arch Otolaryngol Head Neck Surg. 132:1203–1209.

Ishikawa S, Nakayama T, Watanabe M, Matsuzawa T. 2009. Flow mechanisms in the human olfactory groove numerical simulation of nasal physiological respiration during inspiration, expiration, and sniffing. Arch Otolaryngol Head Neck Surg. 135:156–162.

Jiang JB, Zhao K. 2010. Airflow and nanoparticle deposition in rat nose under various breathing and sniffing conditions: a computational evaluation of the unsteady and turbulent effect. J Aerosol Sci. 41:1030–1043.

Keyhani K, Scherer PW, Mozell MM. 1995. Numerical simulation of airflow in the human nasal cavity. J Biomech Eng. 117:429–441.

Keyhani K, Scherer PW, Mozell MM. 1997. A numerical model of nasal odorant transport for the analysis of human olfaction. J Theor Biol. 186: 279–301.

Kurtz DB, Zhao K, Hornung DE, Scherer P. 2004. Experimental and numerical determination of odorant solubility in nasal and olfactory mucosa. Chem Senses. 29:763–773.

Lazar J, Greenwood DR, Rasmussen LEL, Prestwich GD. 2002. Molecular and functional characterization of an odorant binding protein of the Asian elephant, Elephas maximus: implications for the role of lipocalins in mammalian olfaction. Biochemistry. 41:11786–11794.

Linforth RST, Martin F, Carey M, Davidson J, Taylor AJ. 2002. Retronasal transport of aroma compounds. J Agric Food Chem. 50: 1111–1117.

Löbel D, Jacob M, Volkner M, Breer H. 2002. Odorants of different chemical classes interact with distinct odorant binding protein subtypes. Chem Senses. 27:39–44.

Löbel D, Strotmann J, Jacob M, Breer H. 2001. Identification of a third rat odorant-binding protein (OBP3). Chem Senses. 26:673–680.

Marin M, Baek I, Taylor AJ. 1999. Volatile release from aqueous solutions under dynamic headspace dilution conditions. J Agric Food Chem. 47: 4750–4755.

Nespoulous C, Briand L, Delage MM, Tran V, Pernollet JC. 2004. Odorant binding and conformational changes of a rat odorant-binding protein. Chem Senses. 29:189–198.

Pelosi P. 1994. Odorant-binding proteins. Crit Rev Biochem Mol Biol. 29: 199–228.

Pelosi P. 1996. Perireceptor events in olfaction. J Neurobiol. 30:3–19.

Pevsner J, Hou V, Snowman AM, Snyder SH. 1990. Odorant-binding protein—characterization of ligand-binding. J Biol Chem. 265: 6118–6125.

Pevsner J, Sklar PB, Snyder SH. 1986. Odorant-binding protein—localization to nasal glands and secretions. Proc Nat Acad Sci. 83:4942–4946.

Pevsner J, Snyder SH. 1990. Odorant-binding protein: odorant transport function in the vertebrate nasal epithelium. Chem Senses. 15:217–222.

Steinbrecht RA. 1998. Odorant-binding proteins: expression and function. Annals of the New York Academy of Sciences. 855:323–332.

Taylor AJ, Cook DJ, Scott DJ. 2008. Role of odor binding protein: comparing hypothetical mechanisms with experimental data. Chemosens Percept. 1:153–162.

Taylor AJ, Linforth RST. 2003. Direct mass spectrometry of complex volatile and non-volatile flavour mixtures. Int J Mass Spec. 223:179–191.

Walker JKL, Lawson BL, Jennings DB. 1997. Breath timing, volume and drive to breathe in conscious rats: comparative aspects. Respir Physiol. 107: 241–250.

Wiseman T, Williston S, Brandts JF, Lin LN. 1989. Rapid measurement of binding constants and heats of binding using a new titration calorimeter. Anal Biochem. 179:131–137.

Yabuki M, Portman K, Scott D, Briand L, Taylor A. 2010. DyBOBS: a dynamic biomimetic assay for odorant-binding to odor-binding protein. Chemosens Percept. 3:108–117.

Zhao K, Scherer PW, Hajiloo SA, Dalton P. 2004. Effect of anatomy on human nasal air flow and odorant transport patterns: implications for olfaction. Chem Senses. 29:365–379.